Polymer Testing 90 (2020) 106668

Contents lists available at ScienceDirect

Polymer Testing

journal homepage: http://www.elsevier.com/locate/polytest

Shape memory hybrid based on polyvinyl alcohol and 0D silver nanoparticles

José E. Moreno-Marcelino [a], E. Gutierrez-Segura [b], Alfredo R. Vilchis-Nestor [c], Ernestina Castro-Longoria [d], Gustavo López-Téllez [c,*]

[a] Doctorado en Ciencia de Materiales de la Facultad de Química, Universidad Autónoma del Estado de México, Paseo Colón Esquina Paseo Tollocan S/N, Toluca Estado de México, CP, 2250000, Mexico
[b] Facultad de Química, Universidad Autónoma del Estado de México, Paseo Colón Esquina Paseo Tollocan S/N, Toluca Estado de México, CP, 2250000, Mexico
[c] Centro Conjunto de Investigación en Química Sustentable UAEM-UNAM, (CCIQS), Carretera Toluca-Atlacomulco Km 14.5, Unidad El Rosedal, Toluca, Estado de México, CP, 2250200, Mexico
[d] Departamento de Microbiología, Centro de Investigación Científica y de Educación Superior de Ensenada (CICESE), Ensenada, B.C., CP, 22860, Mexico

ARTICLE INFO

Keywords:
Shape memory effect
Silver nanoparticles
Polyvinyl alcohol
Shape memory hybrid

ABSTRACT

Shape memory hybrids (SMH) have drawn significant attention because they allow an easy alternative for the design of shape memory materials with tailored properties or features. In this work, a shape memory hybrid was made, based on polyvinyl alcohol (PVA) as the elastic domain and 0D silver nanoparticles (Agnps) as the transition domain, a dissolution method of mixing both components, and evaporation of water afterward allowed the formation of films of the hybrid material. Two different size distributions of silver nanoparticles were used (13.7 ± 2.6 and 67.9 ± 14.1 nm), in order to study the effect of the size on the shape memory effect (SME) of the final SMH, under temperature stimuli. The materials obtained were characterized using scanning electron microscopy (SEM), transmission electron microscopy (TEM), energy-dispersive X-ray spectroscopy (EDS), X-ray photoelectron spectroscopy, infrared spectroscopy (IR), differential scanning calorimetry (DSC) and thermogravimetric analysis (TGA) techniques. The crystallinity of PVA was slightly altered with the addition of Agnps. Finally, the shape memory effect was tested on both hybrid materials, resulting in a better response to temperature for the SMH prepared with Agnps of 68 nm, also the shape recovery time can be tuned varying both the increase of temperature and the size distribution of Agnps used.

1. Introduction

Generally, the term "smart material" is used to describe materials that are able to respond to external stimuli [1]. Among these, there are shape memory materials (SMM), they are defined as any material that once processed possess a permanent form, but can then be deformed applying an external stimulus, after this stimulus ends the material retains this programmed or deformed shape indefinitely, at least until it is exposed to the same initial stimulus used to deform it in the first place, only that this time the material gradually recovers its original shape. There are several stimuli reported to cause the shape memory effect (SME), such as pressure, pH changes, temperature, contact with solvents, especially water, or even with vapors of them, among others [2]. One of the accepted classifications of SMM is alloys (SMA), polymers (SMP), composites (SMC), and hybrids (SMH) [3]. SMP in particular, have advantages inherent to polymers; simple transition processes, lower density, lower cost, easy processing, among others [4–6]. The SME is based on a dual-domain system, which consists of an elastic domain and a transition domain. Usually for polymers, the SME is produced using an increase in temperature above a "transition temperature" (T_s), afterward the material can be deformed to a programmed shape, which can be maintained indefinitely once the polymer is cooled. The explanation for this phenomenon considers that some energy was stored during the deformation, and the material contains it until it is released, commonly this occurs when temperature is applied, again in an amount equal or higher than T_s, if the programmed shape is not maintained, this is known as shape change capacity [7]. When the polymer reaches T_s it will regain its original or permanent shape, since temperature produces molecular mobility of chain segments, which in turn release the contained energy. Some reports mention that the SME is intrinsically

* Corresponding author.
E-mail address: glopezt@uamex.mx (G. López-Téllez).

https://doi.org/10.1016/j.polymertesting.2020.106668
Received 2 March 2020; Received in revised form 20 May 2020; Accepted 3 June 2020
Available online 10 June 2020

present in polymers, however, in practice, there are some requirements needed for it to occur [2,4,8]. Regarding structure, the material must have net points strong enough so it can "remember" its original shape, these are often but not limited to physical or chemical crosslinking, on the other hand, it must have weaker segments (amorphous or crystalline domains), that allow reversible thermal transition which allows the programming of the polymer [2,8]. These weaker segments are also associated with the glass temperature (T_g), or the melting temperature (T_m).

SMP also have the advantage of a higher deformation percentage (>700%) compared to alloys (>10%), however, there are also some disadvantages such as lower elastic module, limited values in shape recovery, higher response time and a relatively short lifespan [4–6,8]. To overcome these limitations, composites were introduced, SMC as they are known, consist of a polymer matrix and another material dispersed inside it; these dispersed materials often act as reinforcements but they can also improve other properties such as electrical, thermal, and magnetic among others [2,9]. Finally, there are novel materials that also present the SME, and are easier to make in a do-it-yourself manner, known as SMH [3], the main aspect that differentiates SMH from SMC is that the later always have a chemical interaction between the constituents, often via chemical crosslinking, whereas SMH are based on physical interactions, commonly hydrogen bonds, and van der Waals forces. This allows a simple fabrication process, which often consists in selecting two materials with well-known properties needed for the final SMH, the SME in these materials is also based on a dual domain system, an elastic, and a transition domain, the latter is able to change its stiffness when a stimulus is presented. PVA has gathered interest in research as a constituent for SMH since it is biocompatible, biodegradable as it solubilizes in water, it is also easy to process [10–12]. Regarding the processing, it can easily form films, sheets, fibers, and membranes with good mechanical properties [13], and it presents the SME under various stimuli [11,14,15]. There have been many reports of PVA with imbibed materials, for example, Ag [10,16–18], ZnSe [19], Al_2O_3 [14], MWNT [15], among others. Despite reports regarding composites based on PVA with Agnps, they are often focused on antimicrobial activity and testing of electro-optical and mechanical properties [10,16–18]. To the best of our knowledge, there are no reports that evaluate the SME of an SMH made with PVA and Agnps. PVA shape memory properties have been evaluated when Al_2O_3 nanoparticles were added in different weight percentages [14], they found a direct correlation between mechanical properties, and the amount of Al_2O_3 nanoparticles added, this also caused an increase in T_g, however, the crystallinity degree was diminished as seen in the melting peak becoming wider, also diminished was the T_m. The composite displayed a faster recovery towards its original shape when compared to stand-alone PVA. The stimuli used were temperature and solvent exposure. On the other hand, a composite based on PVA and MWNT for shape memory using electrical stimulus has been tested [15], resulting in an increase in T_g as the amount of MWNT increased, also evaluated, was the thermal conductivity of the composite, which is directly correlated to the weight percentage of MWNT inside the polymer matrix, the recovery time was also faster compared to PVA.

Since the literature regarding the effect that Agnps have on the shape memory behavior of PVA is scarce, and considering that silver has a high thermal conductivity, which would allow a better thermal response to trigger the shape memory effect, the objective of this work was to obtain a hybrid material based on PVA and Agnps, using a simple solvent casting technique and evaluating the effect that two different sizes of said nanoparticles have on the shape memory behavior of PVA. The SME was tested using temperature as the stimuli, the tests considered the recovery time and percentage of shape recovery. Also, different amounts of Agnps solution added to PVA, allows the tuning of the response time in shape recovery, which can be suited to different applications. Furthermore, Agnps were synthesized using two different approaches, a chemical and a bioreduction synthesis, showing that the synthesis method of Agnps also has an effect on the final shape memory behavior of PVA.

The hybrid materials were characterized by TEM, SEM, EDS, XPS, FTIR, DSC and TGA analysis.

2. Materials and methods

2.1. Reagents

Polyvinylpyrrolidone (PVP M_W = 10,000), and sodium hydroxide (NaOH, ≥98%), were purchased from Sigma-Aldrich, glucose (glucose D, >99.5%) was provided by Winkler, silver nitrate ($AgNO_3$, >99.3%) was supplied by Fermont. PVA was obtained by hydrolysis of poly (vinyl acetate) in the laboratory of chemistry-engineering (Autonomous University of the State of Mexico). Average M_w 28,000, 87–89% hydrolyzed. All solutions were prepared with distilled water.

2.2. Synthesis of agnps

2.2.1. Chemical synthesis (Ag_Q)

30 mL of glucose 0.1 M solution, 0.3 g of PVP, and 0.15 g of NaOH were added to a bottom flask. With the aid of a hot plate, the solution was heated at 70 °C under stirring (600 rpm). Subsequently, 10 mL of the $AgNO_3$ 0.01 M solution was added at a rate of 200 μL/min with the help of a micropipette; at the end of the addition, stirring was continued for 10 min.

b) Green Chemistry bioreduction Synthesis (Ag_V)

Initially, 80 mL of distilled water was heated in a beaker until boiling. A green tea (*Camellia sinensis*) bag was put in water boiled and it stirred for 5 min at 900 rpm. Immediately 15 mL of *Camellia sinensis* extract was poured into a vial, then 10 mL of $AgNO_3$ 0.01 M solution were added and 35 mL of distilled water to get an overall volume of 60 mL. Finally, the mixture was stirred for 3 h at 800 rpm and preserved at room temperature in glass containers for later use.

2.3. Preparation of hybrid material PVA-Agnps

A PVA 2 %w/v solution was prepared in 10 mL of distilled water, stirred at 1200 rpm and heated at 62 °C for 2 h; simultaneously, 10 mL of the Agnps suspension was sonicated for 10 min. Once PVA was completely dissolved, the hot plate's thermostat was turned off and 10 mL of Agnps solution was added to the PVA solution, and stirred for 15 min. Afterward 10 mL of this mixture were poured in a 30 × 30 × 15 mm polystyrene mold, and it was left at room temperature until complete evaporation of water was achieved, finally, the obtained film was removed from the mold and stored until further use (Scheme 1).

2.4. Evaluation of shape memory effect

Samples evaluated had the following dimensions 31.0 × 8.0 × 0.09 mm. In order to obtain the shape recovery time, films were programmed into two temporal shapes: rolled up and folded. All tests were carried out on a closed system (oven).

Samples were programmed as a rolled-up form and recovery time was determined in function of the temperature. The sample was first heated at 40 °C for 60 s to obtain a programmed shape and afterward cooled at room temperature for 60 s. The temperatures used were in the range of 50–100 °C and evaluated in 10-degree intervals.

Other samples were heated at 80 °C during 60 s to get the folded programmed form and then allowed to cool at room temperature for another 60 s. Finally, a temperature of 100 °C was used to evaluate the recovery percentage (% R) as a function of time according to the following relationship [20]:

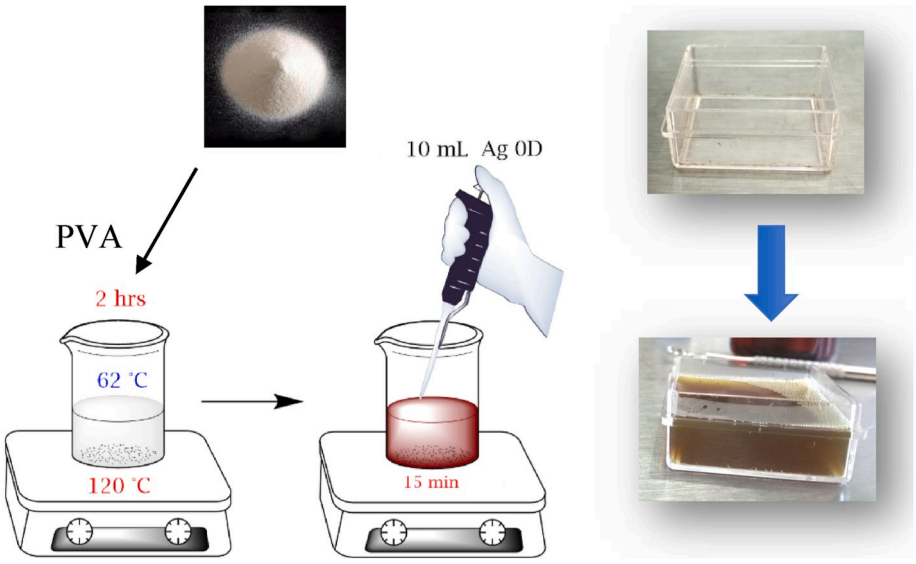

Scheme 1. Obtention of SMH samples.

$$\%R = \left(\frac{\theta_I - \theta_t}{\theta_I}\right)100$$

where θ_I is the deformation angle in the programmed sample, θ_t is the angle at a given time. In order to evaluate the angles, the tests were videotaped, and screenshots were taken at a certain time to evaluate them, with the help of the Android Protractor app® version 1.6.1. For the shape memory cyclic (SMC) test, the previously mentioned methodology was carried out 5 times.

2.5. Characterization of the samples

Uv/Vis absorption spectra were obtained by instrument GENESYS 10S in the range of 300–700 nm in 0.1 nm steps. Infrared spectra of samples were measured with spectrometer Bruker, model TENSOR 27 in the range 4000 to 400 cm^{-1}. XPS spectra were obtained with instrument JEOL model-9200 with a dual source of magnesium, spectra deconvolution was done using software SpecSurf 1.80. TEM images were obtained with an electronic microscope JEOL-2100 with a resolution of 0.23 nm dot by dot and 0.14 nm line by line. Also, the TEM microscope has two STEM detectors: one bright field and an annular dark field. SAED analysis was performed with Crys TBox software version 1.10 [21]. SEM images were obtained by a JEOL-JSM6510LV with secondary and backscattered electron detectors. The microscope is coupled with an EDS BRUKER QUANTAX model 200 with a resolution of ≤129 eV. DSC/TGA analysis was obtained by a thermal analyzer NETZSCH model STA 449 F3 Jupiter, the sample was placed in an aluminum crucible and heated from 40 to 500 °C a heated rate of 10 °C/min in a nitrogen atmosphere (99.999%) was used. Through the use of an ultramicrotome, LEICA ULTRACUT R, ultrathin sections of the hybrid material were obtained and afterward, the dispersion of Agnps in the PVA matrix was evaluated by EDS and STEM analysis. The thin slice sections were placed on carbon-coated Cu grids for analysis.

3. Results and discussion

3.1. Characterization of agnps

3.1.1. UV–Vis spectrophotometry

UV–Vis spectrum absorption of samples Ag_Q and Ag_V are shown in Fig. 1. The reported surface plasmon resonance peak of both samples are characteristic of Ag 0D nanostructures [22,23].

Ag_Q sample presents a single peak with a maximum at 398 nm, which

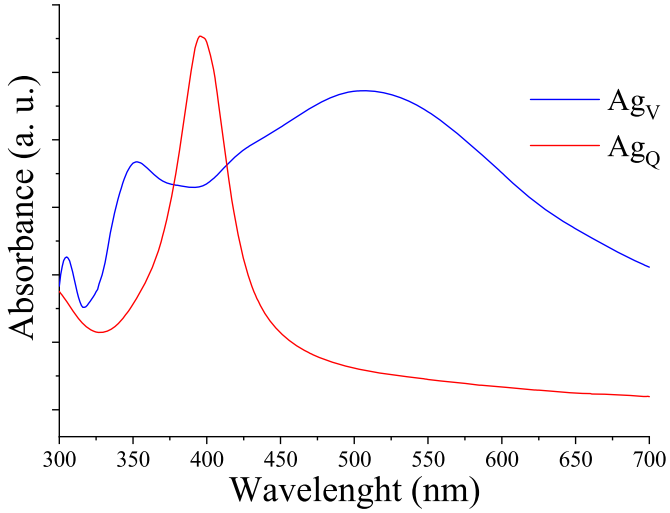

Fig. 1. UV–Vis spectra for samples AgQ, and AgV.

is in good agreement with the reported value; therefore, the shape and size of these nanoparticles must be uniform. The Ag_V sample has two peaks, whose maximum is presented at 507 nm and the other at 353 nm. The pressence of two peaks, as well as their amplitude, may be due to a greater polydispersity of sizes and shapes of Ag nanoparticles [23,24].

Regarding the Ag_Q sample, when adding the first μL of the $AgNO_3$ solution, it quickly presented a yellowish coloration, which implies the rapid formation of nanoparticles. The intensity of coloration is increased from yellow to brown as the reaction time increases, to finally acquire a dark coloration. The role played by glucose is primarily as a solvent for $AgNO_3$, to subsequently reduce the Ag^+ ions to Ag^0 through the oxidation of hydroxyl groups and their subsequent formation of aldehyde groups. For its part, PVP acts as a stabilizer of the nanoparticles, since it prevents uncontrolled growth and agglomeration of these ones [22,25,26].

On the other hand, the Ag_V sample showed the same change in coloration when $AgNO_3$ solution was added, with a gray-green color as the final coloration. In the literature, it is mentioned [24,27] that for those nanoparticles of Ag with very small sizes, the surface plasmon appears around 400 nm. However, as their size increases, the surface plasmon signal shifts towards red, disappearing completely when the

dimensions of the nanostructures surpass the nanometric scale. According to the aforementioned results, we can infer that the size of the nanostructures obtained by this "green" method is of a larger size than those obtained by the chemical method.

Similarly, the role played by the extract of *Camellia sinensis* in the synthesis of nanostructures is to reduce the Ag^{+} ions and later act as a stabilizing agent for the nanostructures [24,28,29]. In general, plant extracts contain various compounds that contribute to the reduction of metal ions, such as terpenoids, polysaccharides, flavonoids, among others [29]. Mainly, terpenoids act as antioxidants in *Camellia sinensis* which is why these compounds contribute to the formation of Agnps [30].

3.1.2. Transmission Electron Microscopy

The characterization by TEM confirms the uniformity of the shape and size of nanoparticles of Ag_Q and uniformity of sizes that exist between the nanostructures (Fig. 2a). Also, quasi-spherical morphologies can be observed which, according to the size distribution analysis (Fig. 2c), showed an average of 13.7 nm ± 2.6 nm. Ag_V sample is shown in Fig. 2d) since OD and 1D morphologies can be observed in them. This may be due to the fact that the shape and size of the nanoparticles depend mainly on the chemical composition of each plant extract used in the synthesis [28].

This type of polydispersity in nanoparticles has already been reported in other investigations [31], even using another type of extract. However, there are already studies that report better control in size and shape [28,32]. Additionally, the analysis of the images allowed us to determine an average size of 67.9 ± 14.1 nm for the nanoparticles (Fig. 2 f); therefore, a larger and wider size distribution of Agnps was obtained in comparison with the Ag_Q sample, as previously suggested by UV–Vis analysis.

Likewise, the SAED pattern of samples Ag_Q and Ag_V (Fig. 2 b) and 2 e), respectively) corroborated the presence of Agnps. The appearance of diffraction rings corresponding to (111), (200), (220) and (311) planes are in good agreement with those reported for face-centered cubic Agnps [10,33,34].

3.1.3. X-ray Photoelectron Spectroscopy

In Fig. 3a, the Ag spectrum for the 3d region of the Ag_Q sample is shown. This region is frequently reported in the literature because it is very sensitive to the chemical changes that occur in the surrounding areas; its analysis provides information to distinguish Ag^{+} from Ag^{0} [27]. The peak at 368.3 eV was assigned to Ag^{0} [18,27,35]. On the other hand, the peak at 367.7 eV corresponds to some interaction between Ag^{0} and oxygen, related to the interaction of Agnps with the carbonyl group of PVP; since as mentioned before, it acts as a stabilizing agent in the formation of nanoparticles, preventing their growth and agglomeration [23,25,26]. Wang et al. [23], mentioned, that nitrogen and oxygen of

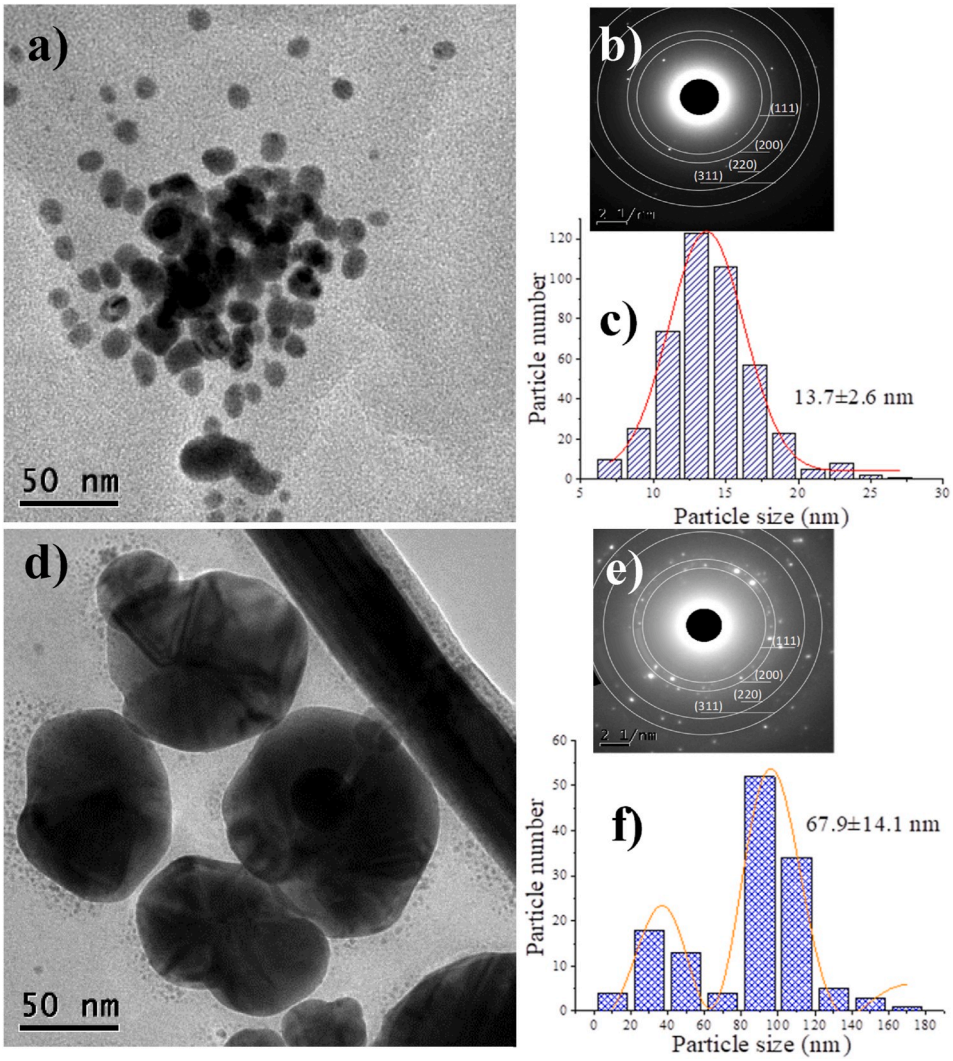

Fig. 2. TEM analysis of Agnps: a)TEM image of AgQ, b)SAED pattern of AgQ and c)Size distribution of AgQ; d)TEM image of AgV, e)SAED pattern of AgV and f)Size distribution of AgV.

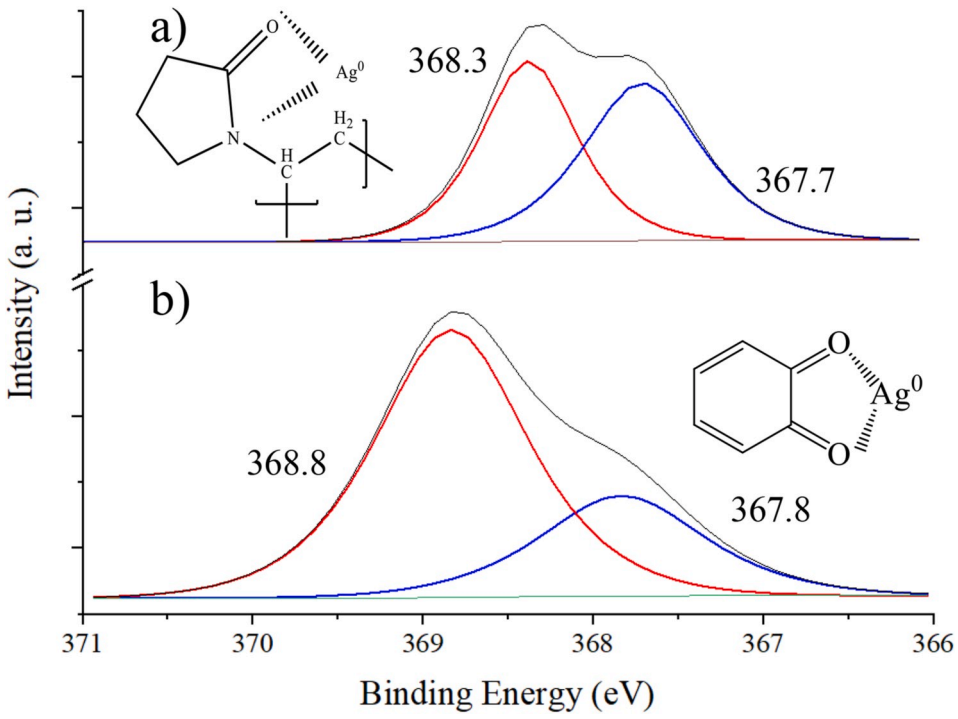

Fig. 3. XPS spectra of samples a) AgQ and b) AgV.

PVP interact with nanoparticles smaller than 50 nm, however, if these are greater than 50 nm the steric effect exerted by both atoms is lost and only oxygen of the carbonyl group acts. Therefore, since the Ag_Q sample has nanoparticles with an average size of 14 nm, it is likely that Agnps interact with both nitrogen and oxygen of the PVP.

Fig. 3b shows the Ag spectrum of the 3d region of the Ag_V sample. Two peaks can be observed, one at 368.8 eV, assigned to Ag^0, and the second at 367.8 eV, assigned to the interaction between Ag^0 and oxygen

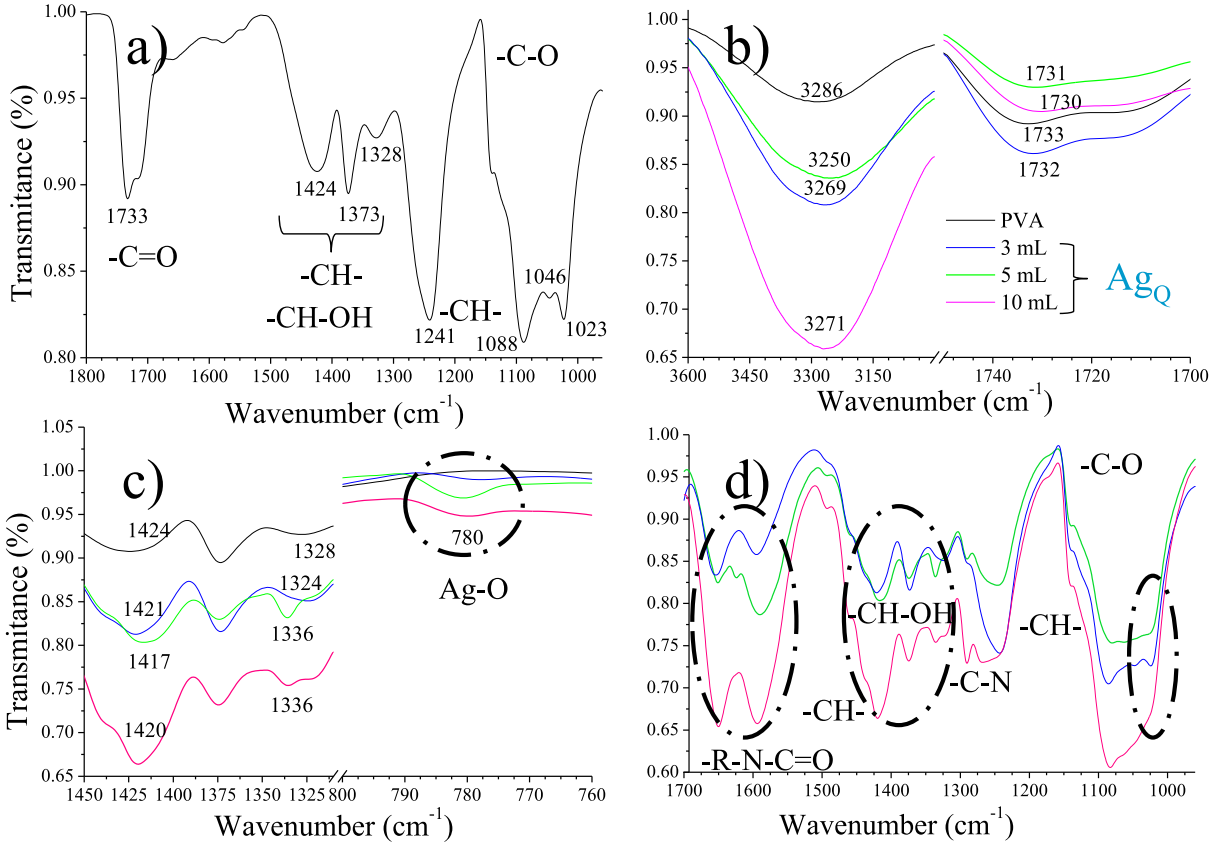

Fig. 4. Infrared spectra of PVA samples: a) Standalone PVA, b), c), and d) close up of selected regions of PVA-Ag_Q.

[18,27,35]. This is due to carbonyl groups present in *Camellia sinensis* that stabilize Agnps [24,28,29].

Furthermore, the ratio between the Ag^0 and Ag interaction peaks in both samples is notable. Clearly, there is a strong interaction between PVP and Ag^0 in the sample Ag_Q. The peak at 367.8 eV and its deconvolution, shows that about 52% of Ag^0 is interacting with the carbonyl group of PVP, and only 27% of the Ag^0 interact with the carbonyl groups of the *Camellia sinensis* in sample Ag_V. As Agnps become bigger the contact surface area diminishes, hence reducing the proportion of silver atoms on the surface which are the ones interacting with oxygen.

3.2. Characterization of hybrid material PVA-Ag 0D

Two types of hybrid materials were prepared from PVA, the first one was called PVA-Ag_Q, which was prepared with the Ag_Q nanoparticles. The second one containing Ag_V nanoparticles was called PVA-Ag_V.

3.2.1. Infrared Spectroscopy

The infrared spectra of PVA and PVA-Ag_Q samples are in Fig. 4. The peak observed in the PVA spectrum (Fig. 4 a)) at 1733 cm^{-1}, corresponds to the vibrations of the –C═O in an ester and is related to the remaining acetate groups from the synthesis (from the hydrolysis of polyvinyl acetate). The peaks observed at 1424, and 1373 cm^{-1}; correspond to the symmetric flexion of $–CH_2$ and out-of-plane flexion of $–CH_2$, respectively. The peak at 1328 cm^{-1} is the result of the combination of frequencies of coupling that exists between the –OH and the –CH groups, The peak at 1241 cm^{-1} corresponds to the out-of-plane flexion of -C-H [16,17,19,36,37]. In addition, between 1087 and 1022 cm^{-1} there are vibrations related to -C-O in alcohols [19,36].

Fig. 4 b) shows a shift towards red and a change in the intensity of the peaks, this is a result of different amounts of Ag_Q added to PVA; the peaks correspond to the vibrations of the bonds –OH (3286 cm^{-1}) and –C═O (1733 cm^{-1}). In contrast, Fig. 4 c) shows that there is an increase in the intensity of the peak corresponding to the $–CH_2$ vibrations at 1424 and 1328 cm^{-1}; so, there is a decoupling of the peaks [16,38,39]. On the other hand, the peak at 1023 cm^{-1} (Fig. 4 d)) decreases its intensity until it disappears completely, this vibration corresponds to the bond stress of –CO, and to the flexion of the –OH bond in PVA [19]. This is caused by a decrement in the interaction between chains, since –OH groups are interacting with Agnps and/or with the –C═O group of PVP. In Fig. 4 d) two peaks can be observed: at 1654 and 1594 cm^{-1}, which correspond to the stress of the bonds of –C═O, and –NC═O of the PVP respectively [40–43]. Wang et al. [23] reported that the –C═O peak of pure PVP appears at 1643 cm^{-1}; so, there is a change in intensity, and a shift from 1643 towards 1654 cm^{-1}, this may be due to the interaction that exists between –C═O and Agnps [23,26,42]. Another relevant aspect is the change in the intensity of the peaks mentioned above; since the increase of intensity is correlated to the volume of Ag_Q added. Despite some works related to similar systems of PVA/nps [19,43,55], there is a lack of discussion regarding the peak below 1600 cm^{-1}. Krumova et al. [44] reported a peak at 1564 cm^{-1} in cross-linked PVA with hexamethylene diisocyanate; which corresponds to the urethane group (R–NH–C═O–O-R′). Likewise, Paul et al. [33] reported that the peak at 1537 cm^{-1} is intensified when Ag nanostructures are added to a polyurethane film; Malina et al. [40] also reported such behavior. Therefore, we consider that the peak at 1594 cm^{-1} observed in Fig. 4 d); corresponds to the formation of hydrogen bonds between –OH groups of PVA and -N-C═O groups of PVP, whose position and intensity are influenced by the presence of the Ag_Q nanoparticles. Finally, a peak can be observed at 780 cm^{-1} (Fig. 6 c) that only appears when adding Ag_Q solution, this

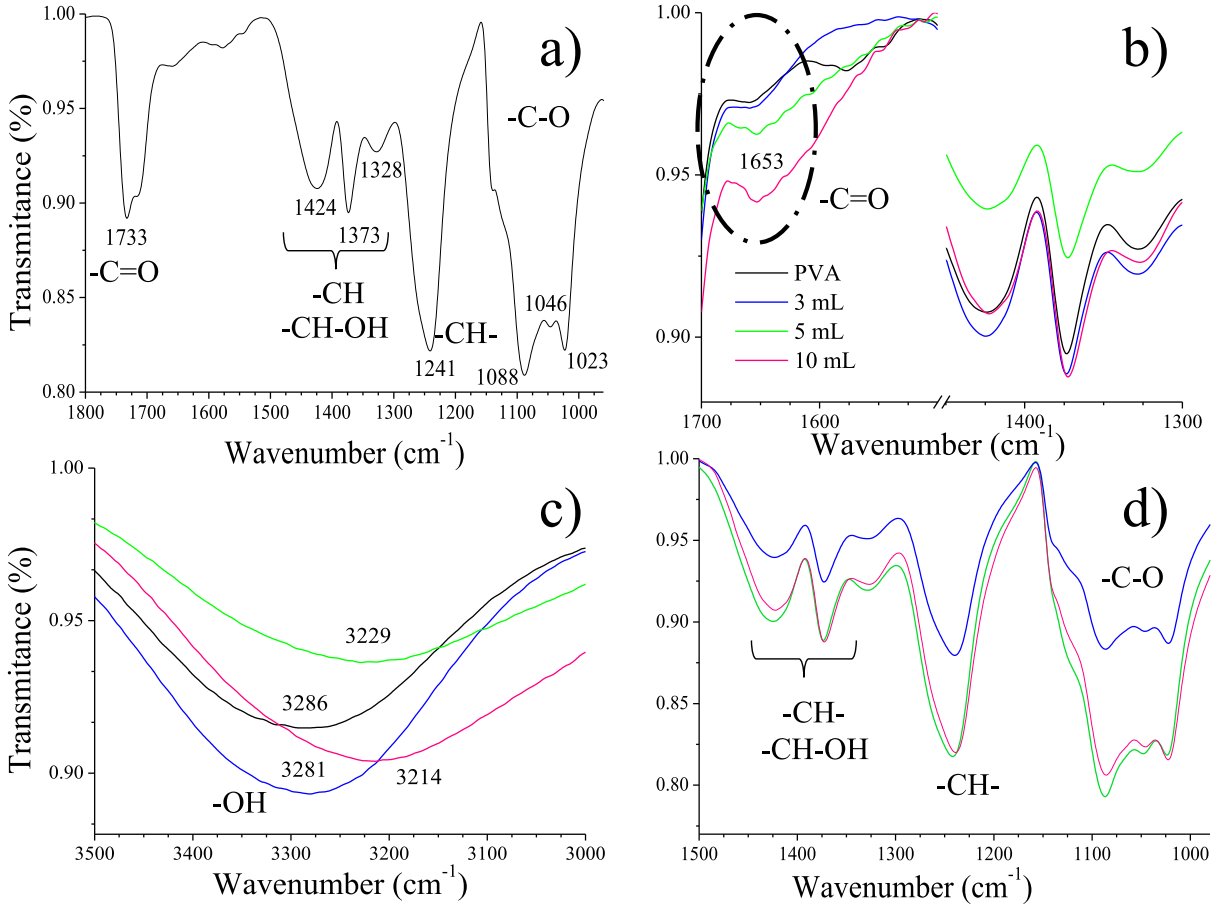

Fig. 5. Infrared spectra of PVA samples: a) Standalone PVA, b), c), and d) close up of selected regions of PVA-AgV.

is reported in the literature [45] as the vibrations of the Ag–O interaction.

Fig. 5 shows the infrared spectra of PVA-Ag_V. No substantial changes are observed with respect to the PVA spectrum since its peaks predominate over the infrared spectrum. There is a change in the coupling between bands at 1328 cm^{-1} and 1424 cm^{-1} [16,36,39]. In addition, there is a shift of the vibrations assigned to the –OH bonds from 3286 towards 3214 cm^{-1}, this change is indicative of the interaction with Agnps. On the other hand, a new peak appears at 1653 cm^{-1}, this has already been reported in other methods of synthesis of nanostructures [46,47], and it is mentioned that it is a result of the interaction between the –C═O group of quinone and the nanostructures. It is well known that gallic acid is one of the main components of plants such as *Camellia sinensis*, and it has been mentioned that it has great properties as an antioxidant [30,46,47]. Additionally, it has been proposed that when gallic acid reduces metallic salts and quinones are formed, these interact with the nanostructures formed by means of –C═O group [46,47]. The previous analysis indicates that there are two interactions between Agnps and PVA in PVA-Ag_V. The first one is with the –OH groups from PVA, while the second interaction is with the –C═O groups of quinone.

3.2.2. *X-ray photoelectron spectroscopy*

To the best of our knowledge, there few works that discuss the possible interactions of the PVA/Agnps system, the closest is the report by Stoyanov [51]. XPS supported with the other techniques described in this work allowed the study of the interactions between components of the hybrids to contribute to the understanding of the role these interactions have with the final shape memory properties.

The XPS analysis of the PVA-Ag_Q sample is shown in Fig. 6. Curve fitting of the C 1s spectra presents 4 peaks (Fig. 6 a). The peak at 287.9 eV may correspond to the –C═O group of either remnant acetate groups (-$COCH_3$) in the PVA or the PVP ring [42,48,49]. On the other hand, the peaks observed at 285.2 and 284.2 eV correspond to PVA and are assigned to the –CH–OH and –CH_2-CH- groups, respectively [48,50]. Finally, the peak at 283.6 eV has been assigned to the metal-carbon-oxygen interaction (Ag–C–O); since, according to the literature, the complex shows a peak below 284 eV for different metals [51]. The deconvolution of O 1s (Fig. 6 b) shows peaks at 529.4 and 530.7 eV corresponding to the Ag–C–O interaction, and the C═O of both PVA and PVP [42,51–53]. On the other hand, the peak at 531.8 eV corresponds to the oxygen bond of –CH–OH [50,52,53]. In general, the peaks are shifted probably due to its interaction with Agnps. The spectrum of Ag (Fig. 6 c), shows two peaks at 368.4 and 369.1 eV, which correspond to the Ag 3d 5/2 region [26,35]. The first peak corresponds to Ag^0, while the second peak corresponds to Ag^0 with some interaction with oxygen [27,54]. These results indicate that the interaction of Agnps in PVA-Ag_Q is mainly with the –C═O group of PVP.

On the other hand, the XPS spectra of the PVA-Ag_V sample is shown in Fig. 7. The C 1s (Fig. 7 a) deconvolution, exhibited 3 peaks: at 288.3 eV the corresponding group is –C═O [52], which according to the infrared analysis may be attributed to the quinone or remnants of acetate groups in PVA. The peaks at 285.2 and 284.2 eV correspond to PVA and are assigned to the –CH–OH and –CH_2-CH- groups respectively [48,50,52].

The O 1s deconvolution (Fig. 7 b)) shows peaks at 533.4, 532.2 and 531.0 eV. The first one corresponds to the C–O–C═O of ethyl acetate, whereas the second one corresponds to the C–OH group both present in PVA [50,52,53]. The peak at 531.0 eV corresponds to the –C═O of quinone [52,53]. The peaks from the interaction between Ag–C–O are not found in C 1s and O 1s deconvolution.

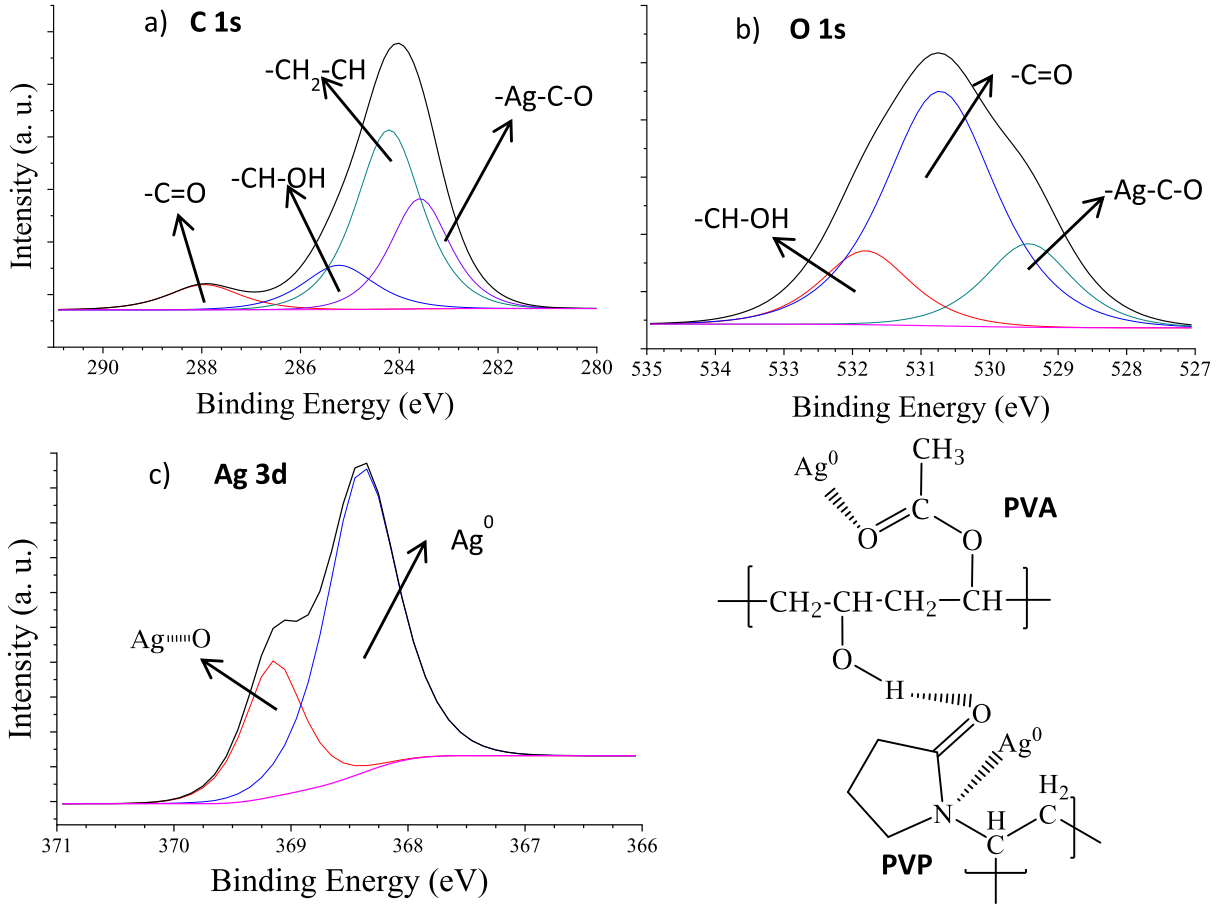

Fig. 6. XPS deconvolution spectra of sample PVA-AgQ. a) C 1s, b) O 1s y c) Ag 3d.

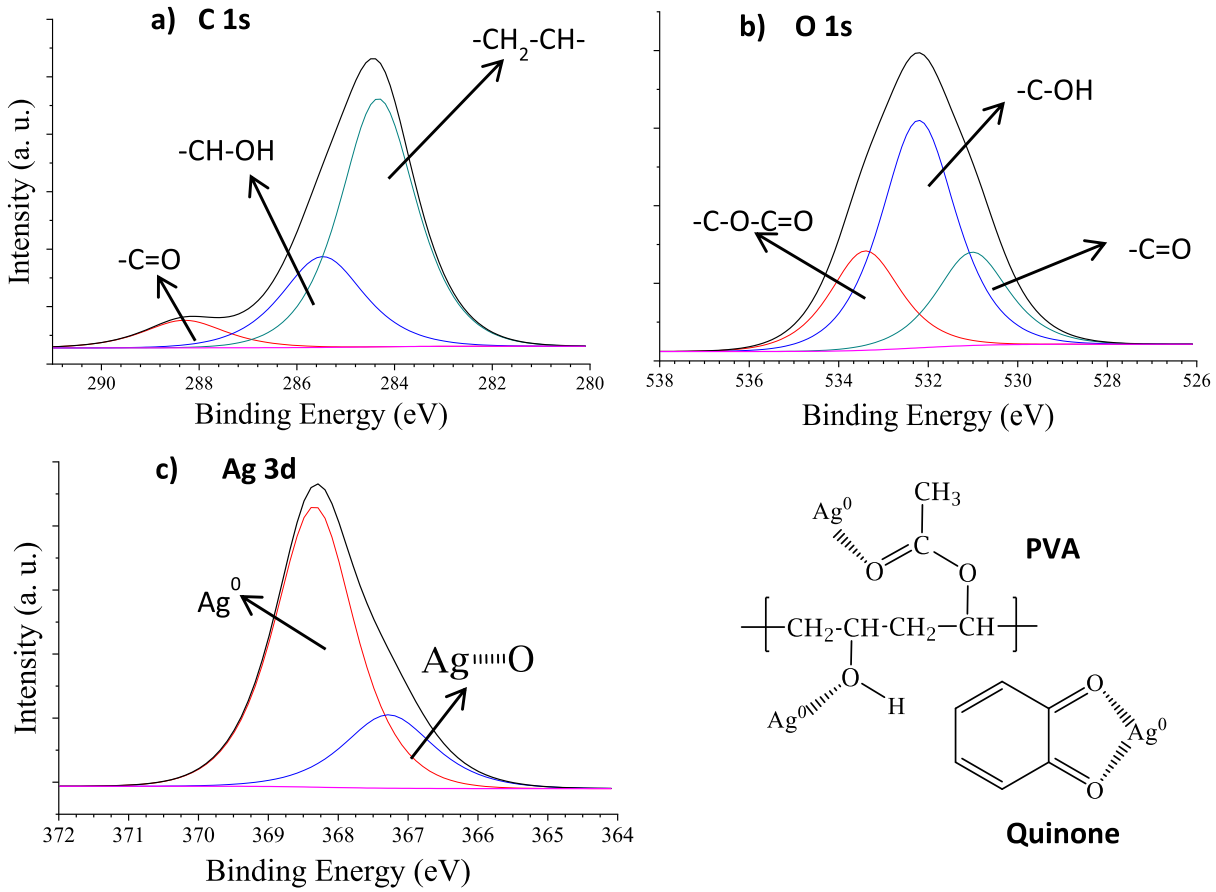

Fig. 7. XPS deconvolution spectra of PVA-AgV. a) C 1s, b) O 1s y c) Ag 3d.

On the other hand, the Ag 3d deconvolution (Fig. 7 b)), shows two peaks at 368.34 eV and 367.28 eV; which are assigned to Ag^0 and Ag^0 interacting with oxygen [27,34,35]. As previously stated, the nanostructures interaction within the sample of PVA-Ag_V is with the oxygen present both in quinone and PVA.

As it can be observed in Figs. 6 and 7, there are different interactions between Ag^0 nanoparticles and PVA, caused mainly by the synthesis method used. The PVP used on the chemical synthesis (Ag_Q) shows a strong interaction with Ag^0 and was corroborated with XPS analysis as well as with FT-IR; therefore, we believe this affects the response time of the PVA-Ag SMH.

The PVA-Ag_Q and PVA-Ag_V corresponding thermograms are shown in Figs. 8 and 9, respectively. The DSC thermograms show pure PVA and PVA-Ag_Q with has different quantities of Ag_Q (Fig. 8). It can be seen that pure PVA's T_g, showed an 80.2 °C value concordant with other studies [13,14,38]. The value of T_g decreases to values between 41.9 and 48.5 °C when different quantities of Ag_Q were added. Such behavior is caused by a decrease in the interactions between the hydrogen bonds of the –OH groups of the polymer chains [13,44,55], having as a consequence more mobility of the chain segments; this was corroborated on the FT-IR and XPS sections. Another factor that contributed to the Tg decrease was due to the high thermal conductivity of Agnps; which provides pathways through PVA improving the thermal conductivity of the hybrid [56]. In spite of this, there are scientific reports of PVA composites with nanoparticles where a T_g increase is present [14,16,38]. The authors indicate that it is the result of direct interactions between the PVA's –OH groups and the respective nanoparticles, giving the chain segments certain stiffness; that is why its T_g increases compared to pure PVA. However, in our hybrid material that interaction is not the same, because it is done mainly by PVP carbonyl groups and not Agnps directly. Additionally, the decomposition temperature (T_d) decreases from 308 to 276.6 °C, as

c) Thermal analysis: DSC/TGA

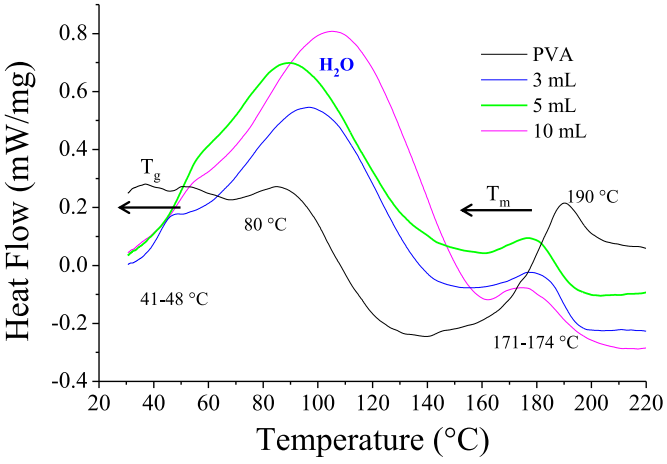

Fig. 8. DSC thermogram of PVA-AgQ.

more volume of Ag_Q is added to PVA; which is a consequence of the same interactions previously stated.

On the other hand, an endothermic peak can also be appreciated at high temperatures, which corresponds to the PVA's crystalline phase T_m, which value is 190.2 °C on pure PVA. A change in peak shape is noticeable as more volume of Ag_Q is used to form the hybrid material, also a shift of T_m values towards lower temperatures (Table 1) occurs and the peak is broadening. Likewise, the crystallinity index (X_C) was determined through the relationship between ΔH_m and ΔH_∞, where

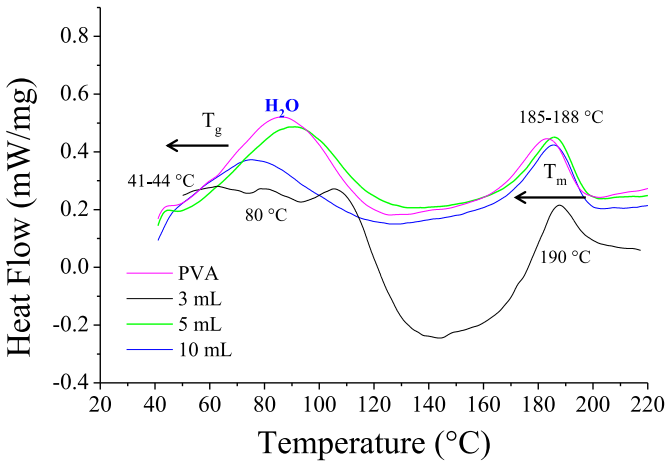

Fig. 9. DSC thermogram of PVA-AgV.

Table 1
ΔH, Tg, Tm and XC values of PVA with different amounts of AgQ or AgV.

Sample	Quantity of nanostructures (mL)	T_g (°C)	T_m (°C)	ΔH_m (J/g)	X_C
PVA	0	80.2	190.2	28.13	19.9
PVA-Ag_Q	3	41.9	174.5	13.13	9.3
	5	48.5	172.6	10.59	7.5
	10	48.4	171.4	9.47	6.7
PVA-Ag_V	3	45.0	188.9	30.67	21.6
	5	41.6	187.4	28.38	20.0
	10	41.3	185.8	27.82	19.6

$\Delta H_\infty = 141.7$ J/g [55,57]; showing the X_C values diminished. Thus, all these results allow us to stipulate that a decrease of the crystalline part of PVA exists as Ag_Q nanoparticles are added; this information corroborates the analysis made by FT-IR and XPS. The observed effects allow us to propose that a structural modification within the PVA exists, in which, Agnps interact within the PVP, incorporating themselves into the PVA's crystalline phase, decreasing crystallinity. At this point, we must also consider the PVP effect on the PVA's crystalline phase decrease; PVP provides interaction points between Agnps and PVA.

In the literature [37,57], it is mentioned that both PVP and PVA have good miscibility, due to interactions via hydrogen bonds between the –C═O groups of PVP and the –OH groups of PVA. Also, DSC characterization of the hybrid materials shows only one T_g and T_m value, this is indicative of the good compatibility that exists between both polymers. The simple fact of mixing the two polymers leads to a decrease of the PVA's crystalline phase which is reflected in the endothermic peak of the same phase; this peak changes its width and its T_m value is shifted toward lower temperatures [43,57].

The PVA-Ag_V thermogram (Fig. 9), shows some similarities in T_g and T_m behavior compared to the PVA-Ag_Q hybrid; however, the reasons for such behavior are different. Even though there is a small decrease in the T_m value (Table 1), its X_C almost remains steady as more volume of Ag_V is added. Mbhele et al. [16] affirmed that this behavior may be caused due to the immobility of PVA chain segments; because the –OH group interacts with Agnps, and according to FT-IR and XPS analysis these interactions are confirmed.

The results indicate that the chain segment distribution was more affected in the hybrid material compared to standalone PVA; due to the reordering of the chain packing caused by interaction with Agnps [16].

In this sense, the T_g decrease may be caused due to the higher thermal conductivity of Agnps; which provide pathways through PVA that improve the thermal conductivity of the hybrid material [56]. Similar results were observed in a hybrid material which also had a T_g decrease, as a consequence of an increase in the mobility of the chain segments due to the presence of filling materials that act as a plasticizer [45]. In our hybrid material, perhaps due to the average size of Agnps (68 nm) they are not within the interstitial spaces of the chains; so, its crystalline phase was not be affected in a great manner [58]. PVA does not show substantial changes in T_d with the added volume of Ag_V from 3 to 10 mL. The T_d values were 321.5, 322.4, and 322.7 °C for 3, 5 and 10 mL of PVA-Ag_V, respectively.

The TGA analysis of PVA-Ag_Q, and PVA-Ag_V hybrids are shown on Fig. 10, a weight loss of 4–6% occurs at around 150 °C in all the samples, this is due to the loss of humidity [59]. The weight loss occurs before 150 °C in PVA-Ag_Q samples, whereas for the PVA-Ag_V samples occurs after 150 °C. The second thermal decomposition occurs at around 220 °C with a weight loss of 3–10%, although this only occurs in PVA-Ag_Q samples. For PVA-Ag_V samples, the second thermal decomposition occurs at 400 °C with a weight loss of 63–69%. This indicates that there is a bigger modification of the PVA chains in PVA-Ag_Q compared to the PVA-Ag_V. This points out to a bigger intermolecular interaction between the Ag_Q nanostructures within the PVA [43].

SEM images of PVA-Ag_Q hybrid are shown in Fig. 11 a) and 11 b). It can be observed an almost homogeneous and porous surface, with a small agglomeration of nanostructures distributed on the sample. By means of EDS analysis (Fig. 11 b), and chemical mapping, the homogeneous distribution of Agnps was confirmed with a 15.96 wt % of silver.

Fig. 11c) and d) shows SEM images of PVA-Ag_V, they present a homogeneous material, with some porosity and a homogeneous distribution of Agnps, with a 10.20% weight of silver (Fig. 11 d).

Fig. 12 shows TEM/STEM images of PVA-Ag_Q, it can be observed that there is a homogenous distribution of Agnps at different magnifications; there are not noticeable agglomerations. By means of STEM/EDS line-scan analysis, the presence of Ag on the PVA-Ag_Q hybrid is corroborated.

The shape memory effect evaluated by the obtained hybrids (PVA-Ag_Q and PVA-Ag_V) is depicted in Fig. 13. The hybrid materials demonstrated good shape memory, the samples recovered its permanent shape almost completely.

First, the samples were programmed into a cylindrical rolled shape. The shape recovery rate in terms of applied temperature showed different behaviors for PVA-Ag_Q and PVA-Agv hybrids. In both materials, the results revealed that the recovery time decreased with increasing the temperature (Fig. 14). For instance, better recovery times for the PVA sample indicated the following order: 5.4 s (100 °C) > 6.8 s (80 °C) > 18 s (50 °C). On the other hand, the recovery time for PVA-Ag_Q is different than the times for PVA and PVA-Agv in each temperature evaluated; at 80 °C is 10.6, 6.8 and 3.8 s, respectively.

The recovery time on folded programmed shape was studied for PVA, PVA-Ag_V and PVA-Ag_Q and are shown in Fig. 15. It can be seen that PVA-Ag_Q hybrid has a slower recovery time than PVA-Ag_V and PVA, besides PVA and PVA-Ag_V have similar values of recovery times. The shape memory presents a sigmoidal behavior [20] and was evaluated through a regression slope of data samples. The equation slope was $0.7868x - 78.33$, $1.091x - 68.82$, and $1.0835x - 43.07$ for PVA-Ag_Q, PVA-Ag_V and PVA, with a determination coefficient of 0.98, 0.94 and 0.98 respectively. The response time was slightly better (0.7%) in PVA-Ag_V than PVA, whereas, it diminished 19% for PVA-Ag_Q compared to that of PVA.

Consequently, the recovery time was improved by adding Agnps and better reproducibility of the tests was obtained when using a programmed cylindrical rolled-up deformation. According to different studies [15,60,61], the thermal conductivity on materials with the SME effect is closely related to the recovery time. In the case of polymer composites, thermal conductivity depends on some factors [62,63] such as crystallinity of the polymer matrix, morphology, nature of the embedded particles inside the matrix, distribution of particles, etc.

One of the main requirements to increase thermal conductivity, is the homogeneous distribution of nanoparticles, which was obtained in both hybrids and corroborated by SEM, TEM, STEM and EDS analysis. Agnps homogenous distribution produces thermal conduction networks which

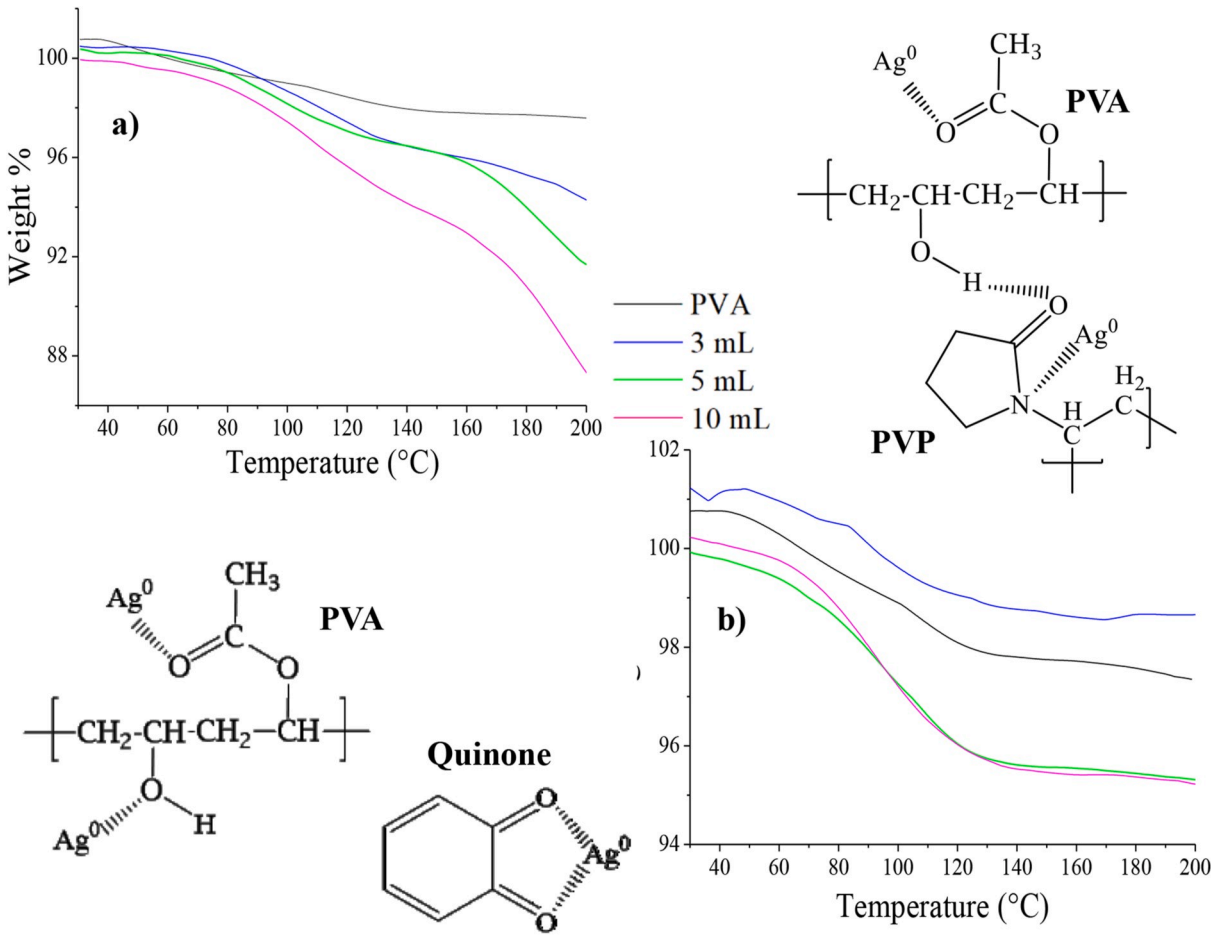

Fig. 10. TGA thermograms of hybrid composites: a) PVA-AgQ and b) PVA-AgV.

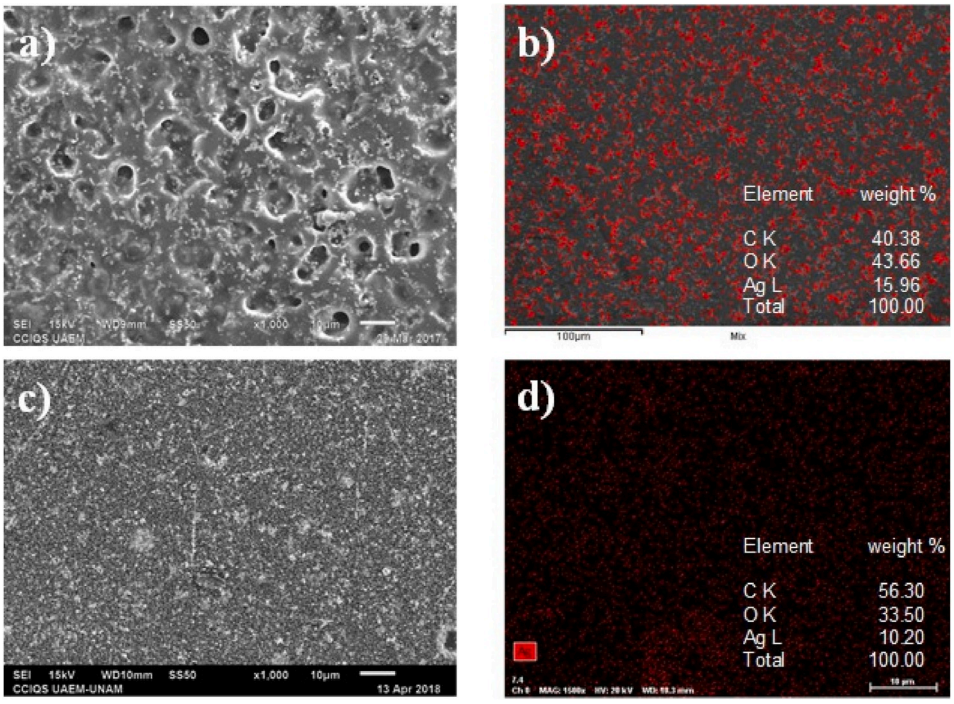

Fig. 11. SEM/EDS analysis of PVA-AgQ hybrid (a and b) and PVA-Agv hybrid (c, and d).

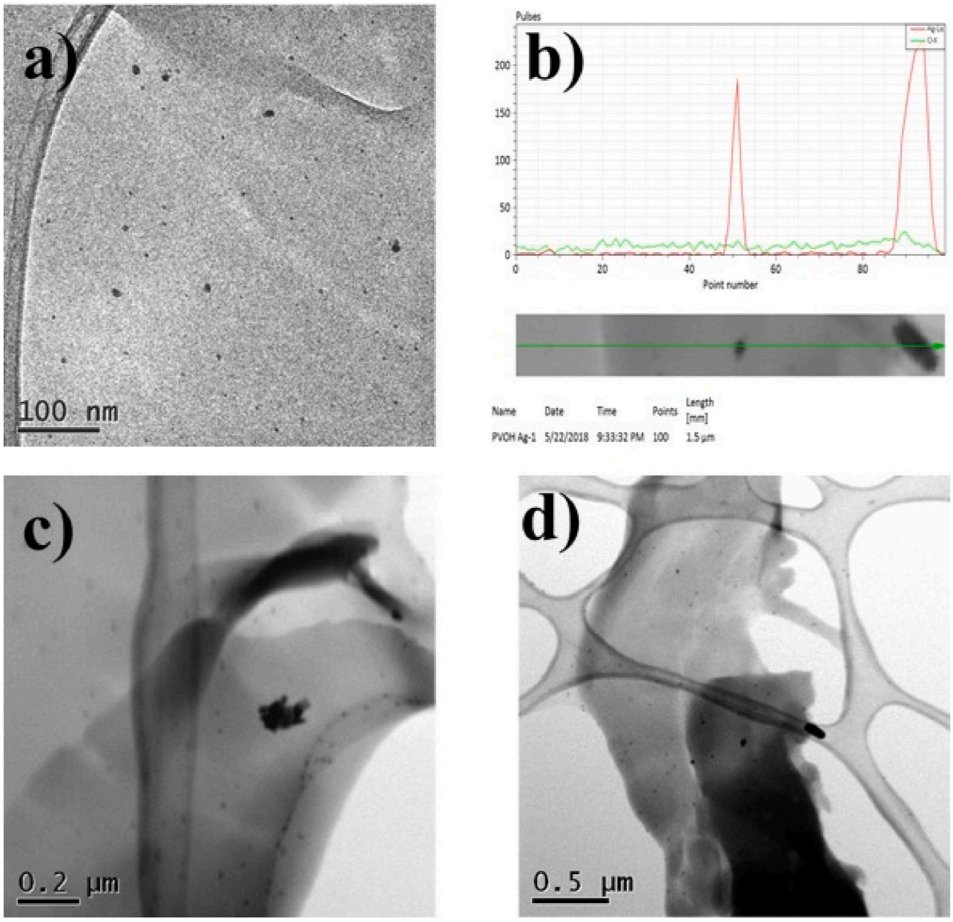

Fig. 12. Image analysis of thin slices of PVA-AgQ hybrid: a), c) and d) TEM images at different magnifications, b) STEM-Bright Field.

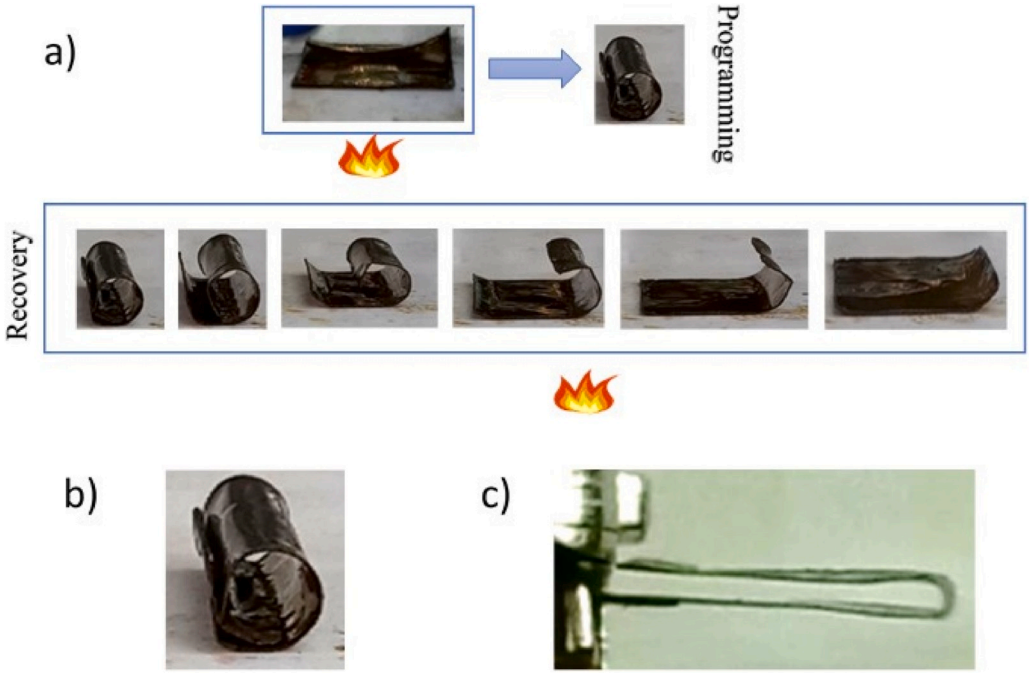

Fig. 13. a) General shape memory process in obtained hybrid composites, examples of programmed shape: b) rolled up and c) folded.

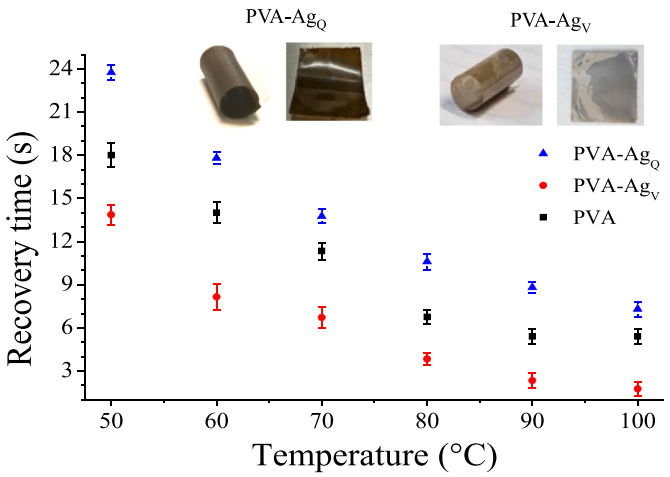

Fig. 14. Recovery time of PVA and hybrid materials.

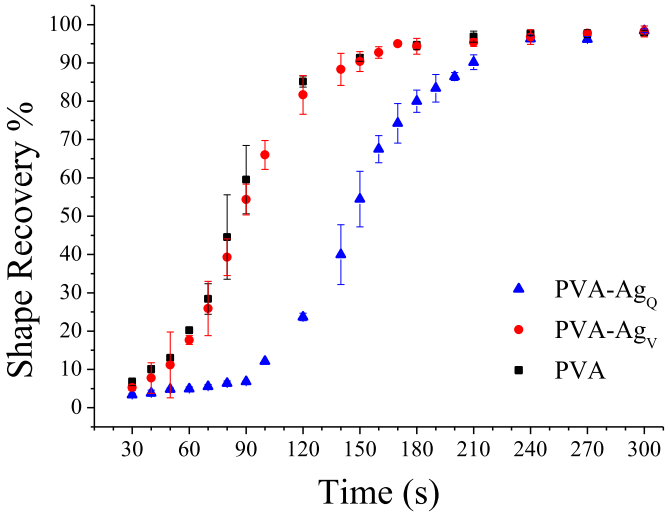

Fig. 15. Thermally shape recovery of hybrid materials, % of recovery vs response time.

in turn increase the thermal conductivity throughout the material [15,58,64]. Likewise, the size and shape of the nanoparticles have a great influence over the thermal conductivity [5,63,65,66]. Warrier et al. [66], reported that thermal conductivity has a behavior proportional to the size of the nanoparticles when the size of the nanoparticles is decreased the thermal conductivity decreased as well; due to the way in which the nanoparticles are bonded.

Additionally, small nanoparticles have a bigger contact area than larger nanoparticles, so their contact resistance is increased and this has an influence on the electrons scattering, having, as a result, a low thermal conductivity. On the other hand, as the size of the nanoparticles increases, the contact resistance is way lower, inferring a higher thermal conductivity [5,66].

Agnps in PVA-Ag$_Q$ hybrid are smaller than those present in PVA-Ag$_V$ hybrid, influencing the shape recovery time and thus, the thermal conductivity; causing a better response time for PVA-Ag$_V$. Therefore, although there is a thermal conductivity network in both hybrids, the size of the nanoparticles had a greater influence on the shape recovery time. Also, PVP had a great influence on the shape recovery rate due to its interaction with Agnps.

$T_g = 41$ °C
$T_g = 48$ °C

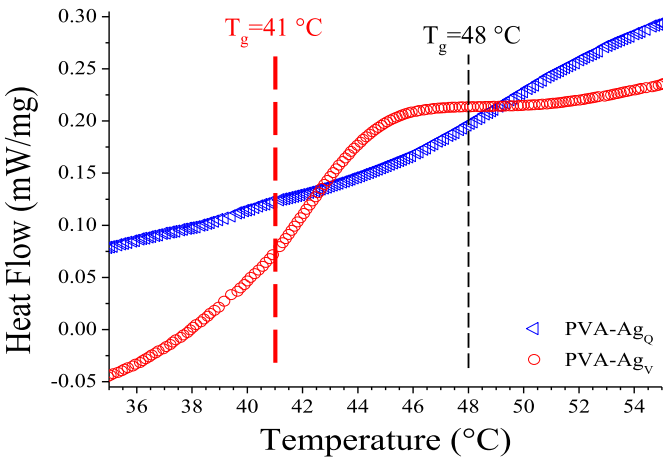

Fig. 16. DSC thermograms of hybrid materials: Transition range of Tg.

A side effect of adding nanoparticles in PVA is a decrease in interactions between chain segments, which increases their mobility and decrease T_g values [43,56,58,64]. Fig. 16 shows the glass temperature range (T_g) of PVA-Ag$_V$ and PVA-Ag$_Q$ hybrids. In terms of the dynamics of polymer chains, it is evident that the transition range of PVA-Ag$_V$ is narrower than PVA-Ag$_Q$. Babaahmadi et al. [61], found that polymers with shape memory and a wide T_g transition interval, have a slower recovery rate. Furthermore, he found that the narrowing of the transition zone is a signal of improvement in thermal conductivity. On the other hand, as observed on the thermal analysis, there was a diminishment of the crystalline phase when Agnps were added in PVA-Ag$_Q$; whereas on PVA-Ag$_V$ the crystalline phase was almost steady. The literature states that those polymers who have a higher presence of crystalline phase, have better thermal conductivity due to a bigger mean free path of the phonon when compared with a higher amount of amorphous phase [5,63,67,68].

Therefore, PVA-Ag$_V$ has better thermal conductivity than PVA-Ag$_Q$, which is due to the presence of a homogeneous distribution of Agnps on PVA, as well as their larger size and possible interactions with –OH groups from PVA, causing a narrower T_g transition zone and a lesser PVA crystalline phase perturbation. Finally, PVA-Agv shows better shape recovery times than PVA-Ag$_Q$. A similar finding was reported for other polymer composites [15,20,60,61]. Bai et al. [14] reported recovery times of 33 s using a temperature of 90 °C, for a system consisting of PVA/Al_2O_3 nanoparticles, contrasting with recovery times of PVA/Agnps hybrids of this work of less that 10 s, these faster recovery times could be due to the better thermal conductivity of silver nanoparticles, and possibly a better distribution. They also reported recoveries above 95%. Du et al. [15] reported recovery times of 35 s using electricity for a PVA/MWNTs system, which is still slower than the recovery times observed in our PVA/Agnps system, additionally their results where performed using a 20 wt% of MWNTs, with lower percentages requiring higher voltages.

3.2.3. *Shape memory cyclic (SMC)*

SMC tests are shown in Fig. 17. The shape recovery percentage has fluctuations of 1% when cycle tests were carried out in all samples. Overall PVA-Ag$_Q$ and PVA samples seem to have less fluctuations than PVA-Ag$_V$ but all of them are in the range of 1% of change along the cycles. These results show that the hybrids can withstand 5 cycles and still present an acceptable shape recovery, similar to that of PVA. Regarding recovery times PVA tends to increase its recovery times from 270 s to 300 s, this represents a 10% increase on recovery time, in comparison the hybrids present different behaviors depending on the amount of Agnps added, for 3 mL PVA-Ag$_V$ shows slower recovery times after the second cycle ending with about 16% slower recovery times,

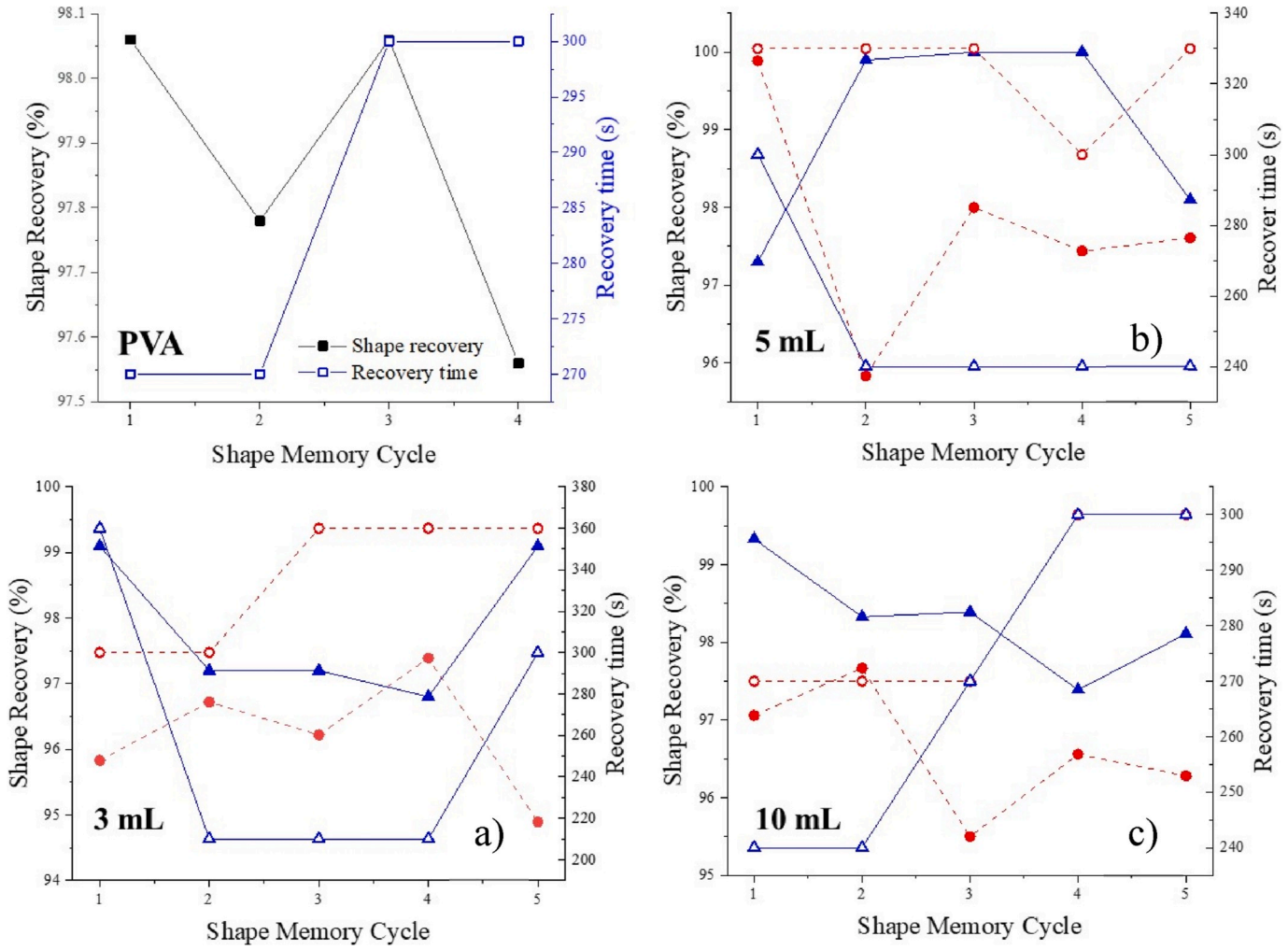

Fig. 17. SMC of hybrid samples with a) 3 mL, b) 5 mL and c) 10 mL. Solid and hollow symbols correspond to shape recovery and recovery time, respectively. PVA-Ag_V correspond to circle symbol whereas PVA-Ag_Q correspond to triangle symbol.

PVA-Ag_Q however actually diminishes its recovery time after the first cycle, with about 41% faster times, after the fourth cycle it increases to 300 s, which is still faster than the original time of 360 s, this could be due to the greater modification of the polymer network compared to that of PVA-Ag_V that was corroborated in previous characterization. For 5 mL of Agnps added, PVA-Ag_V has a slight variation in the fourth cycle with a decrease in the recovery time of 30 s, but for the fifth cycle it returns to its original time of 330 s, overall it can be said that it maintains its recovery times, PVA-Ag_Q however shows faster recovery times after the first cycle and stabilizes after the second cycle, overall it would represent a 20% faster recovery time. Finally for 10 mL of Agnps added, both hybrids tend to increase their recovery times, both ending after the fifth cycle with a recovery time identical to that of PVA (300 s), these differences in recovery times must be related to the degree of modification of the polymer network, and also the distribution of Agnps, however further tests are necessary to accurately relate the factors affecting these differences.

4. Conclusion

An SMH was successfully obtained in a very easy way by mixing PVA in an aqueous solution with a colloidal solution of Agnps, these nanoparticles were synthesized using two methods: bioreduction with *Camellia sinensis* extract, which resulted in Agnps with an average size of 68 nm, and chemical reduction, using PVP as capping agent, producing Agnps with an average size of 14 nm. The size of Agnps as well as the synthesis method used have a great influence on the PVA's shape memory behavior. PVP from the chemical synthesis interacts with Agnps according to the FT-IR and XPS analysis, as well as with the crystalline structure of PVA according to the DSC-TGA analysis. Therefore, by affecting the crystalline phase, the Agnps effectiveness on the thermal conductivity decreases, which causes a slower recovery time when compared to PVA. On the other hand, Agnps obtained by bioreduction showed a better recovery time; because the crystalline phase of the polymeric matrix was not affected, having as a result, an efficient thermal conductivity generated by Agnps.

Besides, it was observed that increasing the temperature results in faster recovery times. Finally, there was better reproducibility on the shape memory experiments when the programmed form was a cylindrical rolled-up shape, attaining recovery values of 95%, and response times of 3.8 s at 80 °C or less than 1.5 s when using 100 °C, this represents an improvement in the recovery speed up to 55% when compared with PVA, besides the results indicate that it is possible to tune the recovery rate by using Agnps with different sizes, and also with the temperature used to trigger the SME. Regarding SMC tests, the recovery percentage has average fluctuations of 1% after 5 cycles for the hybrids which is similar to that of PVA. For the recovery time the amount of Agnps added has an effect on recovery times, PVA-Ag_V tends to get slower recovery times and PVA-Ag_Q tends to get faster recovery times at 3 and 5 mL of Agnps added, for 10 mL of Agnps added both hybrids tend to get slower recovery times but after the fifth cycle they end with the same times (300 s) as PVA. These could allow the tuning of

recovery times for specific applications, however. further testing is necessary to determine the effect several cycles have on recovery times and the factors affecting them.

Declaration of competing interest

None.

CRediT authorship contribution statement

José E. Moreno-Marcelino: Methodology, Validation, Formal analysis, Investigation, Writing - original draft, Visualization. **E. Gutierrez-Segura:** Resources, Validation. **Alfredo R. Vilchis-Nestor:** Investigation, Funding acquisition, Resources. **Ernestina Castro-Longoria:** Methodology, Investigation. **Gustavo López-Téllez:** Conceptualization, Methodology, Validation, Resources, Writing - review & editing, Supervision, Project administration, Funding acquisition.

Acknowledgment

We gratefully acknowledge M. C. Alejandra Núñez Pineda and M. C. Lizbeth Triana Cruz for DSC/TGA and FT-IR technical support respectively. To the laboratory of chemical-engineering UAEM for the supply of PVA reagent. This research was financially supported by CONACYT Grant No. 280518 and Grant A1-S-34533.

Appendix A. Supplementary data

Supplementary data related to this article can be found at https://doi.org/10.1016/j.polymertesting.2020.106668.

References

[1] Z.G. Wei, R. Sandstrom, S. Miyazaki, Review Shape memory materials and hybrid composites for smart systems Part II Shape-memory hybrid composites, J. Mater. Sci. 33 (1998) 3743–3762.
[2] F. Pilate, A. Toncheva, P. Dubois, J.M. Raquez, Shape-memory polymers for multiple applications in the materials world, Eur. Polym. J. 80 (2016) 268–294, https://doi.org/10.1016/j.eurpolymj.2016.05.004.
[3] W.M. Huang, Z. Ding, C.C. Wang, J. Wei, J. Zhao, H. Purnawali, Shape memory materials, Mater. Today 13 (2010) 54–61, https://doi.org/10.1016/B978-0-323-37127-8.00014-5.
[4] T. Pretsch, Review on the functional determinants and durability of shape memory polymers, Polymers 2 (2010) 120–158, https://doi.org/10.3390/polym2030120.
[5] H. Chen, V.V. Ginzburg, J. Yang, Y. Yang, W. Liu, Y. Huang, L. Du, B. Chen, Thermal conductivity of polymer-based composites: fundamentals and applications, Prog. Polym. Sci. 59 (2016) 41–85, https://doi.org/10.1016/j.progpolymsci.2016.03.001.
[6] Q. Meng, J. Hu, A review of shape memory polymer composites and blends, Compos. Part A Appl. Sci. Manuf. 40 (2009) 1661–1672, https://doi.org/10.1016/j.compositesa.2009.08.011.
[7] W.M. Huang, Y. Zhao, C.C. Wang, Z. Ding, H. Purnawali, C. Tang, J.L. Zhang, Thermo/chemo-responsive shape memory effect in polymers: a sketch of working mechanisms, fundamentals and optimization, J. Polym. Res. 19 (2012), https://doi.org/10.1007/s10965-012-9952-z.
[8] I.A. Rousseau, Challenges of shape memory Polymers : a review of the progress toward overcoming SMP ' s limitations, Polym. Eng. Sci. (2008) 2075–2089, https://doi.org/10.1002/pen.21213.
[9] B.Q.Y. Chan, Z.W.K. Low, S.J.W. Heng, S.Y. Chan, C. Owh, X.J. Loh, Recent advances in shape memory soft materials for biomedical applications, ACS Appl. Mater. Interfaces 8 (2016) 10070–10087, https://doi.org/10.1021/acsami.6b01295.
[10] I. Saini, J. Rozra, N. Chandak, S. Aggarwal, P.K. Sharma, A. Sharma, Tailoring of electrical, optical and structural properties of PVA by addition of Ag nanoparticles, Mater. Chem. Phys. 139 (2013) 802–810, https://doi.org/10.1016/j.matchemphys.2013.02.035.
[11] H. Du, J. Zhang, Solvent induced shape recovery of shape memory polymer based on chemically cross-linked poly(vinyl alcohol), Soft Matter 6 (2010) 3370–3376, https://doi.org/10.1039/b922220k.
[12] M. Mohsin, A. Hossin, Y. Haik, Thermal and mechanical properties of poly(vinyl alcohol) plasticized with glycerol, J. Polym. Sci. 122 (2011) 3102–3109, https://doi.org/10.1002/app.
[13] J.-S. Park, J.-W. Park, E. Ruckenstein, On the viscoelastic properties of poly(vinyl alcohol) and chemically crosslinked poly(vinyl alcohol), J. Appl. Polym. Sci. 82 (2001) 1816–1823, https://doi.org/10.1002/app.2023.
[14] Q. Bai, G. Zhang, B. Xu, X. Feng, H. Jiang, H. Li, Thermal and water dual-responsive shape memory poly(vinyl alcohol)/Al2O3 nanocomposite, RSC Adv. 5 (2015) 91213–91217, https://doi.org/10.1039/C5RA17103B.
[15] F.P. Du, E.Z. Ye, W. Yang, T.H. Shen, C.Y. Tang, X.L. Xie, X.P. Zhou, W.C. Law, Electroactive shape memory polymer based on optimized multi-walled carbon nanotubes/polyvinyl alcohol nanocomposites, Compos. B Eng. 68 (2015) 170–175, https://doi.org/10.1016/j.compositesb.2014.08.043.
[16] Z.H. Mbhele, M.G. Salemane, C.G.C.E. Van Sittert, J.M. Nedeljković, V. Djoković, A.S. Luyt, Fabrication and characterization of silver-polyvinyl alcohol nanocomposites, Chem. Mater. 15 (2003) 5019–5024, https://doi.org/10.1021/cm034505a.
[17] M. Ghanipour, D. Dorranian, Effect of Ag-nanoparticles doped in polyvinyl alcohol on the structural and optical properties of PVA films, J. Nanomater. 2013 (2013) 1–10, https://doi.org/10.1155/2013/897043.
[18] S. Lin, R.-Z. Wang, Y. Yi, L.-M. Hao, J.-H. Wu, Hu He, Facile and green fabrication of electrospun poly (vinyl alcohol) nanofibrous mats doped with narrowly dispersed silver nanoparticles, Int. J. Nanomed. 9 (2014) 3937–3947.
[19] S.K. Muntaz Begum, K. Ravindranadh, R.V.S.S.N. Ravikumar, M.C. Rao, Spectroscopic studies on PVA capped ZnSe nanoparticles, Optoelectron. Adv. Mater. Rapid Commun. 10 (2016) 889–892.
[20] X. Luo, P.T. Mather, Conductive shape memory nanocomposites for high speed electrical actuation, Soft Matter 6 (2010) 2146–2149, https://doi.org/10.1039/c001295e.
[21] M. Klinger, More features, more tools, more CrysTBox, J. Appl. Crystallogr. 50 (2017) 1226–1234, https://doi.org/10.1107/S1600576717006793.
[22] V.K. Sharma, R.A. Yngard, Y. Lin, Silver nanoparticles: green synthesis and their antimicrobial activities, Adv. Colloid Interface Sci. 145 (2009) 83–96, https://doi.org/10.1016/j.cis.2008.09.002.
[23] H. Wang, X. Qiao, J. Chen, X. Wang, S. Ding, Mechanisms of PVP in the preparation of silver nanoparticles, Mater. Chem. Phys. 94 (2005) 449–453, https://doi.org/10.1016/j.matchemphys.2005.05.005.
[24] M. Ahamed, M.A. Majeed Khan, M.K.J. Siddiqui, M.S. Alsalhi, S.A. Alrokayan, Green synthesis, characterization and evaluation of biocompatibility of silver nanoparticles, Phys. E Low-Dimensional Syst. Nanostructures. 43 (2011) 1266–1271, https://doi.org/10.1016/j.physe.2011.02.014.
[25] N.L. Pacioni, C.D. Borsarelli, V. Rey, A. V Veglia, Synthetic routes for the preparation of silver nanoparticles: a mechanistic perspective, in: E. Alarcon, M. Griffith, K.I. Udekwu (Eds.), Silver Nanoparticle Appl. Fabr. Des. Med. Biosensing Devices, 2015, pp. 13–46, https://doi.org/10.1007/978-3-319-11262-6.
[26] A. Mirzaei, K. Janghorban, B. Hashemi, M. Bonyani, Characterization and optical studies of PVP-capped silver nanoparticles, J. Nanostructure Chem. 7 (2017) 37–46, https://doi.org/10.1007/s40097-016-0212-3.
[27] Y.W.O.O. Kim, D.O.K. Lee, K.J.U. Lee, B.R. Min, J.H.A.K. Kim, In situ formation of silver nanoparticles within an amphiphilic graft copolymer film, J. Polym. Sci., Part B: Polym. Phys. 45 (2007) 1283–1290, https://doi.org/10.1002/polb.
[28] A.K. Mittal, Y. Chisti, U.C. Banerjee, Synthesis of metallic nanoparticles using plant extracts, Biotechnol. Adv. 31 (2013) 346–356, https://doi.org/10.1016/j.biotechadv.2013.01.003.
[29] I. Siavash, Green synthesis of metal nanoparticles using plants, Grenn Chem. 13 (2011) 2638–2650, https://doi.org/10.1039/c1gc15386b.
[30] A.R. Vilchis-Nestor, V. Sánchez-Mendieta, M.A. Camacho-López, R.M. Gómez-Espinosa, M.A. Camacho-López, J.A. Arenas-Alatorre, Solventless synthesis and optical properties of Au and Ag nanoparticles using Camellia sinensis extract, Mater. Lett. 62 (2008) 3103–3105, https://doi.org/10.1016/j.matlet.2008.01.138.
[31] J. Huang, Q. Li, D. Sun, Y. Lu, Y. Su, X. Yang, H. Wang, Y. Wang, W. Shao, N. He, J. Hong, C. Chen, Biosynthesis of silver and gold nanoparticles by novel sundried Cinnamomum camphora leaf, Nanotechnology 18 (2007), https://doi.org/10.1088/0957-4484/18/10/105104.
[32] P. Raveendran, J. Fu, S.L. Wallen, Completely "green" synthesis and stabilization of metal nanoparticles, J. Am. Chem. Soc. 125 (2003) 13940–13941, https://doi.org/10.1021/ja029267j.
[33] D. Paul, S. Paul, N. Roohpour, M. Wilks, P. Vadgama, Antimicrobial, mechanical and thermal studies of silver particle-loaded polyurethane, J. Funct. Biomater. 4 (2013) 358–375, https://doi.org/10.3390/jfb4040358.
[34] H.J. Li, A.Q. Zhang, Y. Hu, L. Sui, D.J. Qian, M. Chen, Large-scale synthesis and self-organization of silver nanoparticles with Tween 80 as a reductant and stabilizer, Nanoscale Res. Lett. 7 (2012) 1–13, https://doi.org/10.1186/1556-276X-7-612.
[35] A.M. Ferraria, A.P. Carapeto, A. Maria, X-ray photoelectron spectroscopy : silver salts revisited, Vacuum 86 (2012) 1988–1991, https://doi.org/10.1016/j.vacuum.2012.05.031.
[36] A.S. Kutsenko, V.M. Granchak, Photochemical synthesis of silver nanoparticles in polyvinyl alcohol matrices, Theor. Exp. Chem. 45 (2009) 300–305.
[37] O. Şanli, E. Orhan, G. Asman, Release of salicylic acid through poly(vinyl alcohol)/poly(vinyl pyrrolidone) and poly(vinyl alcohol-g-N-vinyl-2-pyrrolidone) membranes, J. Appl. Polym. Sci. 102 (2006) 1244–1253, https://doi.org/10.1002/app.24453.
[38] A. Nimrodh Ananth, S. Umapathy, J. Sophia, T. Mathavan, D. Mangalaraj, On the optical and thermal properties of in situ/ex situ reduced Ag NP's/PVA composites and its role as a simple SPR-based protein sensor, Appl. Nanosci. 1 (2011) 87–96, https://doi.org/10.1007/s13204-011-0010-7.
[39] P.K. Khanna, N. Singh, S. Charan, V.V.V.S. Subbarao, R. Gokhale, U.P. Mulik, Synthesis and characterization of Ag/PVA nanocomposite by chemical reduction method, Mater. Chem. Phys. 93 (2005) 117–121, https://doi.org/10.1016/j.matchemphys.2005.02.029.

[40] D. Malina, A. Sobczak-Kupiec, Z. Wzorek, Z. Kowalski, Silver nanoparticles synthesis with different concentrations of polyvinylpyrrolidone, Dig. J. Nanomater. Biostructures. 7 (2012) 1527–1534.
[41] G.G. Suchkova, L.I. Maklakov, Amide bands in the IR spectra of urethanes, Vib. Spectrosc. 51 (2009) 333–339, https://doi.org/10.1016/j.vibspec.2009.09.002.
[42] Y. Zhang, J.-Y. Liu, S. Ma, Y.-J. Zhang, X. Zhao, X.-D. Zhang, Z.-D. Zhang, Synthesis of PVP-coated ultra-small Fe3O4 nanoparticles as a MRI contrast agent, J. Mater. Sci. Mater. Med. 21 (2010) 1205–1210, https://doi.org/10.1007/s10856-009-3881-3.
[43] I.S. Elashmawi, H.E. Abdel Baieth, Spectroscopic studies of hydroxyapatite in PVP/PVA polymeric matrix as biomaterial, Curr. Appl. Phys. 12 (2012) 141–146, https://doi.org/10.1016/j.cap.2011.05.011.
[44] M. Krumova, D. López, R. Benavente, C. Mijangos, J.M. Pereña, Effect of crosslinking on the mechanical and thermal properties of poly (vinyl alcohol), Polymer 41 (2000) 9265–9272.
[45] M. Abdelaziz, E.M. Abdelrazek, Effect of dopant mixture on structural, optical and electron spin resonance properties of polyvinyl alcohol, Phys. B Condens. Matter 390 (2007) 1–9, https://doi.org/10.1016/j.physb.2006.07.067.
[46] S. Naz, A.R. Khaskheli, A. Aljabour, H. Kara, F.N. Talpur, S.T.H. Sherazi, A. A. Khaskheli, S. Jawaid, Synthesis of highly stable cobalt nanomaterial using gallic acid and its application in catalysis, Adv. Chem. 2014 (2014) 1–6, https://doi.org/10.1155/2014/686925.
[47] W. Wang, Q. Chen, C. Jiang, D. Yang, X. Liu, S. Xu, One-step synthesis of biocompatible gold nanoparticles using gallic acid in the presence of poly-(N-vinyl-2-pyrrolidone), Colloids Surfaces A Physicochem. Eng. Asp. 301 (2007) 73–79, https://doi.org/10.1016/j.colsurfa.2006.12.037.
[48] J.M. Ino, P. Chevallier, D. Letourneur, D. Mantovani, C. Le Visage, Plasma functionalization of poly(vinyl alcohol) hydrogel for cell adhesion enhancement, Biomatter 3 (2013), e25414, https://doi.org/10.4161/biom.25414.
[49] C.Y. Tang, Y. Kwon, J.O. Leckie, Effect of membrane chemistry and coating layer on physiochemical properties of thin film composite polyamide RO and NF membranes I. FTIR and XPS characterization of polyamide and coating layer chemistry, DES 242 (2009) 149–167, https://doi.org/10.1016/j.desal.2008.04.003.
[50] P. Louette, F. Bodino, J.-J. Pireaux, Poly(vinyl alcohol) (PVA) XPS reference core level and energy loss spectra, Surf. Sci. Spectra 12 (2005) 106–110, https://doi.org/10.1116/11.20050922.
[51] P. Stoyanov, S. Akhter, J.M. White, XPS study of metal/polymer interaction: evaporated aluminum on polyvinyl alcohol polymer, Surf. Interface Anal. 15 (1990) 509–515, https://doi.org/10.1002/sia.740150903.
[52] H. Yang, S. Xu, L. Jiang, Y. Dan, Thermal decomposition behavior of poly (vinyl alcohol) with different hydroxyl content, J. Macromol. Sci. Part B Phys. 51 (2012) 464–480, https://doi.org/10.1080/00222348.2011.597687.
[53] T. Zhao, R. Sun, S. Yu, Z. Zhang, L. Zhou, H. Huang, R. Du, Size-controlled preparation of silver nanoparticles by a modified polyol method, Colloids Surfaces A Physicochem. Eng. Asp. 366 (2010) 197–202, https://doi.org/10.1016/j.colsurfa.2010.06.005.
[54] S. Lin, R.-Z. Wang, Y. Yi, L.-M. Hao, J.-H. Wu, Hu He, Facile and green fabrication of electrospun poly(vinyl alcohol) nanofibrous mats doped with narrowly dispersed silver nanoparticles, Int. J. Nanomed. 9 (2014) 3937–3947.
[55] S. Clémenson, L. David, E. Espuche, Structure and morphology of nanocomposite films prepared from polyvinyl alcohol and silver nitrate: influence of thermal treatment, J. Polym. Sci. Part A Polym. Phys. 45 (2007) 2657–2672, https://doi.org/10.1002/pola.
[56] J.B. González-Campos, E. Prokhorov, I.C. Sanchez, J.G. Luna-Bárcenas, A. Manzano-Ramrez, J. González-Hernndez, Y. López-Castro, R.E. Del Río, Molecular dynamics analysis of PVA-AgnP composites by dielectric spectroscopy, J. Nanomater. (2012) 1–11, https://doi.org/10.1155/2012/925750.
[57] Y. Nishio, T. Haratani, T. Takahashi, Miscibility and orientation behavior of blends, J. Polym. Sci., Part B: Polym. Phys. 28 (1990) 355–376.
[58] S. Mahendia, a.K. Tomar, S. Kumar, Electrical conductivity and dielectric spectroscopic studies of PVA–Ag nanocomposite films, J. Alloys Compd. 508 (2010) 406–411, https://doi.org/10.1016/j.jallcom.2010.08.075.
[59] H. Awada, C. Daneault, Chemical modification of poly(vinyl alcohol) in water, Appl. Sci. 5 (2015) 840–850, https://doi.org/10.3390/app5040840.
[60] C. Liu, P.T. Mather, A shape memory polymer with improved shape recovery *, Mater. Res. Soc. 855 (2005) 1–6.
[61] M. Babaahmadi, M. Sabzi, G.R. Mahdavinia, M. Keramati, Preparation of amorphous nanocomposites with quick heat triggered shape memory behavior, Polymer 112 (2017) 26–34, https://doi.org/10.1016/j.polymer.2017.01.074.
[62] A. Tessema, D. Zhao, J. Moll, S. Xu, R. Yang, C. Li, S.K. Kumar, A. Kidane, Effect of filler loading, geometry, dispersion and temperature on thermal conductivity of polymer nanocomposites, Polym. Test. 57 (2017) 101–106, https://doi.org/10.1016/j.polymertesting.2016.11.015.
[63] Z. Han, A. Fina, Thermal conductivity of carbon nanotubes and their polymer nanocomposites: a review, Prog. Polym. Sci. 36 (2011) 914–944, https://doi.org/10.1016/j.progpolymsci.2010.11.004.
[64] A. Gautam, S. Ram, Preparation and thermomechanical properties of Ag-PVA nanocomposite films, Mater. Chem. Phys. 119 (2010) 266–271, https://doi.org/10.1016/j.matchemphys.2009.08.050.
[65] L. Rivière, A. Lonjon, E. Dantras, C. Lacabanne, P. Olivier, N.R. Gleizes, Silver fillers aspect ratio influence on electrical and thermal conductivity in PEEK/Ag nanocomposites, Eur. Polym. J. 85 (2016) 115–125, https://doi.org/10.1016/j.eurpolymj.2016.08.003.
[66] P. Warrier, A. Teja, Effect of particle size on the thermal conductivity of nanofluids containing metallic nanoparticles, Nanoscale Res. Lett. 6 (2011) 247, https://doi.org/10.1186/1556-276X-6-247.
[67] W.N. Dos Santos, J.A. De Sousa, R. Gregorio, Thermal conductivity behaviour of polymers around glass transition and crystalline melting temperatures, Polym. Test. 32 (2013) 987–994, https://doi.org/10.1016/j.polymertesting.2013.05.007.
[68] I. Krupa, I. Novák, I. Chodák, Electrically and thermally conductive polyethylene/graphite composites and their mechanical properties, Synth. Met. 145 (2004) 245–252, https://doi.org/10.1016/j.synthmet.2004.05.007.